

Pontryagin Neural Operator for Solving General-Sum Differential Games with Parametric State Constraints

Lei Zhang[†]

Mukesh Ghimire[†]

Zhe Xu[†]

Wenlong Zhang[‡]

Yi Ren[†]

LZHAN300@ASU.EDU

MGHIMIRE@ASU.EDU

XZHE1@ASU.EDU

WENLONG.ZHANG@ASU.EDU

YIREN@ASU.EDU

[†] Department of Mechanical and Aerospace Engineering, Arizona State University, Tempe, AZ, 85287, USA

[‡] School of Manufacturing Systems and Networks, Arizona State University, Mesa, AZ, 85212, USA.

Abstract

The values of two-player general-sum differential games are viscosity solutions to Hamilton-Jacobi-Isaacs (HJI) equations. Value and policy approximations for such games suffer from the curse of dimensionality (CoD). Alleviating CoD through physics-informed neural networks (PINN) encounters convergence issues when value discontinuity is present due to state constraints. On top of these challenges, it is often necessary to learn generalizable values and policies across a parametric space of games, e.g., for game parameter inference when information is incomplete. To address these challenges, we propose in this paper a Pontryagin-mode neural operator that outperforms existing state-of-the-art (SOTA) on safety performance across games with parametric state constraints. Our key contribution is the introduction of a costate loss defined on the discrepancy between forward and backward costate rollouts, which are computationally cheap. We show that the discontinuity of costate dynamics (in the presence of state constraints) effectively enables the learning of discontinuous values, without requiring manually supervised data as suggested by the current SOTA. More importantly, we show that the close relationship between costates and policies makes the former critical in learning feedback control policies with generalizable safety performance.

Keywords: Differential Games, Physics-informed Neural Network, Pontryagin Neural Operator

1. Introduction

We consider two-player differential games with general-sum, deterministic dynamics, state constraints, and complete information. The Nash equilibrium values of such games satisfy a set of Hamilton-Jacobi-Isaacs (HJI) equations (Crandall and Lions, 1983). It is well known that approximating values and policies of differential games suffers from the following challenges: Firstly, alleviating the curse of dimensionality (CoD) through physics-informed neural networks (PINN) encounters convergence issues when value discontinuity or large Lipschitz constant is present due to state constraints (Zhang et al., 2023a): for system states and time starting from which a constraint cannot be satisfied eventually, the value becomes infinite (or large with constraints are treated as penalties). Secondly, for policies to have good safety performance with respect to the state constraints, we need not only small approximation error for values but also for the gradients of values with respect to the states (Yu et al., 2022). Lastly, it is often necessary to learn generalizable values and policies across a parametric space of games, e.g., for the inference of game parameters when such information is private (Cardaliaguet, 2012). In this paper we focus on parameters that define large penalties that represent state constraints.

To address these challenges, we propose Pontryagin neural operator (PNO). PNO addresses the first and second challenges by introducing and minimizing costate losses defined on the discrepancy between forward and backward costate and value dynamics following Pontryagin’s Maximum Principle (PMP) (Mangasarian, 1966): First, the costate dynamics that reflect state constraint violation can be readily computed by an ODE solver, and serves as a Lagrangian-frame self-supervised signal to facilitate the learning of highly nonlinear values, which cannot be achieved by the standard Eulerian-frame PINN. Second, the direct connection between costates and policies through the Hamiltonian makes costate-based learning more effective at converging to the ground-truth policies. For the last challenge on generalization to parametric PDEs, we extend our costate-based PINN from solving a single HJI equation to parametric HJIs using a DeepONet architecture (Lu et al., 2021), a neural operator that supports point-wise value gradient predictions needed for closed-loop control.

Contributions. (1) **Convergence without supervision:** The convergence issue in solving discontinuous HJI values via PINN has been investigated in (Zhang et al., 2023a), where the authors proposed to hybridize PINN using supervised equilibria data generated by solving games offline via PMP with sampled initial states. The major limitation of the hybrid method is in its assumption that knowledge already exists regarding where the informative equilibria should be sampled in the vast state space, e.g., collision and near-collision cases in vehicle interactions. In addition, generating supervisory data via solving PMP encounters numerical and convergence issues due to the existence of multiple equilibria and singular arcs. To the best of the authors’ knowledge, this paper is among the first to address this convergence issue *without* using any supervised data or domain knowledge of corner cases. To do so, we sample costate trajectories based on a sampling distribution defined over the state space, which evolves along the training according to the costate loss landscape. Considering costate losses as PMP-driven constraints, the sampling distribution essentially captures the dual variables of the PINN. We conduct numerical studies using a two-vehicle game at an uncontrolled intersection. Our experimental results reveal that, with the same data complexity, PNO surpasses the hybrid method in safety performance across a range of parametric collision zones. (2) **Solving parametric HJI via value decomposition:** This paper is also among the first to study the efficacy of physics-informed neural operators in the context of HJI equations. We show that the DeepONet architecture essentially learns a decomposition of the parametric value and identifies the major value basis functions. Empirical results on the same two-vehicle game show that the safety performance of the learned neural operator across a parametric set of collision zones closely aligns with the ground truth. This investigation opens up new directions towards explainable data-driven models for policy learning: Can we translate basis value (or costate) functions into explainable sub-policies (e.g., temporal logic rules) that together comprise generalizable policies for parametric sets of games?

2. Related Work

Differential games with state constraints. The existence of value for zero-sum differential games with Markovian payoffs and state constraints (and temporal logic specifications in general) have been derived (Fisac et al., 2015). The results have been extended to general-sum games with non-temporal state constraints (Pérolat et al., 2017). To facilitate value approximation using level set methods, an epigraphical technique has been introduced to smooth discontinuous values when state constraints are present (Gammoudi and Zidani, 2023).

HJI equations and physics-informed neural networks (PINN). HJI equations resulted from differential games are first-order nonlinear PDEs that suffer from CoD when solved by conventional level set methods (Osher et al., 2004; Mitchell and Templeton, 2005) or essentially nonoscillatory schemes (Osher and Shu, 1991). Monte Carlo methods, such as variants of PINN (Krishnapriyan et al., 2021), have recently shown promise at solving high-dimensional PDEs, including HJ equations, provided that the solution is smooth (Weinan et al., 2021). PINN uses a trainable neural net to represent the solution space, and optimizes PDE-driven errors to approximate the solution. Such errors include the boundary residual (Han and Long, 2020; Han et al., 2018), the PDE residual (Jagtap et al., 2020; Bansal and Tomlin, 2021), and supervisory data on the characteristic curves of the PDE (Nakamura-Zimmerer et al., 2021). Convergence and generalization of PINN have been analyzed under the assumption that both the solution and the network are Lipschitz continuous (Han and Long, 2020; Shin et al., 2020; Ito et al., 2021). Recent studies have explored the effectiveness of PINN for solving PDEs with discontinuous solutions (Jagtap et al., 2020) and solutions with large Kolmogorov n -width (Mojgani et al., 2023). However, solving PDEs with discontinuous solutions and only terminal boundaries (such as HJI equations with state constraints) is still an open challenge without prior structural knowledge about the value landscape (Zhang et al., 2023b).

Neural operators. Neural operators emerged as a promising approach to universally approximating mappings between functions (Kovachki et al., 2023), with particularly successful applications to solving parametric PDEs (Wang et al., 2021). The architecture most related to this paper is DeepONet (Lu et al., 2021), which is composed of a branch net and a trunk net. The branch net extracts informative features of discretized input functions that define parameters of PDEs and the trunk net captures the basis functions that comprise parametric PDE solutions. DeepONet is one of the neural operator architectures that allow point-wise prediction, instead of predicting the entire function over its input domain (e.g., FNO (Li et al., 2020) and GNOT (Hao et al., 2023)). The extension of neural operators from supervised to PINN training has been studied for solving parametric physics equations defined on 2D and 3D state spaces (Wang et al., 2021). This paper examines the efficacy of the DeepONet architecture in physics-informed training of values with large Lipschitz constants defined on a 5D state-time space and a 2D parameter space.

3. Differential Games with State Constraints

Notations and assumptions. Let the state dynamics of Player i be $\dot{x}_i = f_i(x_i, u_i)$, where $x_i \in \mathcal{X}_i \subseteq \mathbb{R}^{d_x}$ is the system state and $u_i \in \mathcal{U}_i \subseteq \mathbb{R}^{d_u}$ is the control input. The joint state space is $\mathcal{X} := \mathcal{X}_1 \times \mathcal{X}_2$. The instantaneous loss of Player i is denoted by $l_i(\cdot, \cdot) : \mathcal{X} \times \mathcal{U}_i \rightarrow \mathbb{R}$ and the terminal loss $g_i(\cdot) : \mathcal{X}_i \rightarrow \mathbb{R}$. The fixed time horizon of the game is $[0, T]$. We use $\mathbf{a}_i = (a_i, a_{-i})$ to concatenate elements a_i from Player i and a_{-i} from the fellow player, and use $\mathbf{a} = (a_1, a_2)$. Denote $\alpha_i \in \mathcal{A} : \mathcal{X} \times [0, T] \rightarrow \mathcal{U}_i$ as Player i 's policy. We use $x_s^{x_i, t, \alpha_i}$ as the state of Player i at time s if it follows policy α_i , dynamics f_i , and starts at (x_i, t) . $\mathbf{x}_s^{x_i, t, \alpha_i} := (x_s^{x_i, t, \alpha_i}, x_s^{x_{-i}, t, \alpha_{-i}})$. Let $c_i(\cdot) : \mathcal{X} \rightarrow \mathbb{R}$ be a state penalty derived from Player i 's state constraints, i.e., for any $\mathbf{x}_i \in \mathcal{X}$, $c_i(\mathbf{x}_i) = 0$ if \mathbf{x}_i satisfies Player i 's state constraints, and otherwise $c_i(\mathbf{x}_i)$ becomes a large positive number. In this paper, we consider $c_i(\cdot)$ to be differentiable but with a large Lipschitz constant. The value of Player i is denoted by $\vartheta_i(\cdot, \cdot) : \mathcal{X} \times [0, T] \rightarrow \mathbb{R}$. We omit arguments to f_i , l_i , g_i , c_i , ϑ_i when possible, and decorate them with the superscript $\theta \in \Theta \subseteq \mathbb{R}^{d_\theta}$ when the corresponding functions are type-specific, where Θ is the type space. E.g., $c_i^\theta(\cdot, \cdot)$ is the state penalty of Player i

of type θ . Throughout the paper, we assume that \mathcal{U}_i is compact and convex; f_i and c_i are Lipschitz continuous; l_i and g_i are Lipschitz continuous and bounded.

Value and HJI with state constraints. Let α^\dagger be a pair of equilibrium policies of the payoffs

$$J_i(\mathbf{x}_i, t, \alpha_i) := \int_t^T (l_i(\mathbf{x}_s^{\mathbf{x}_i, t, \alpha_i}, \alpha_i(\mathbf{x}_s^{\mathbf{x}_i, t, \alpha_i}, s)) + c_i(\mathbf{x}_s^{\mathbf{x}_i, t, \alpha_i})) ds + g_i(\mathbf{x}_T^{\mathbf{x}_i, t, \alpha_i}) \quad (1)$$

for $i \in \{1, 2\}$, so that

$$J_i(\mathbf{x}_i, t, \alpha_i^\dagger) \leq J_i(\mathbf{x}_i, t, (\alpha_i, \alpha_{-i}^\dagger)), \quad \forall \alpha_i \in \mathcal{A}, \quad \forall i \in \{1, 2\}. \quad (2)$$

The value for Player i is $\vartheta_i(\mathbf{x}_i, t) = J_i(\mathbf{x}_i, t, \alpha_i^\dagger)$. The HJI equations that govern the values are denoted by L , and the boundary conditions by D (Starr and Ho, 1969):

$$\begin{aligned} L(\vartheta_i, \nabla_{\mathbf{x}_i} \vartheta_i, \mathbf{x}_i, t) &:= \nabla_t \vartheta_i + \max_{u \in \mathcal{U}_i} \{ \nabla_{\mathbf{x}_i} \vartheta_i^T \mathbf{f}_i - (l_i + c_i) \} = 0 \\ D(\vartheta_i, \mathbf{x}_i) &:= \vartheta_i(\mathbf{x}_i, T) - g_i = 0, \quad \forall i = 1, 2. \end{aligned} \quad (3)$$

By solving Eq. (3) for $(\vartheta_1, \vartheta_2)$, Player i 's equilibrium policy can be derived as

$$\alpha_i^\dagger(\mathbf{x}_i, t) = \arg \max_{u \in \mathcal{U}_i} \{ \nabla_{\mathbf{x}_i} \vartheta_i^T \mathbf{f}_i - (l_i + c_i) \}.$$

When needed, we denote by $\mathcal{L}^\theta := (L^\theta, D^\theta)$ the HJI of a game parameterized by θ .

Method of characteristics. The characteristic curves of \mathcal{L} are open-loop equilibrium trajectories governed by PMP: For initial state $(\bar{x}_1, \bar{x}_2) \in \mathcal{X}$ and $t \in [0, T]$:

$$\begin{aligned} \dot{x}_i &= f_i, \quad x_i(t) = \bar{x}_i, \\ \dot{\lambda}_i &= -\nabla_{x_i} (\lambda_i^T \mathbf{f}_i - (l_i + c_i)), \quad \lambda_i(T) = -\nabla_{x_i} g_i, \\ u_i &= \arg \max_{u \in \mathcal{U}_i} \{ \lambda_i^T \mathbf{f}_i - (l_i + c_i) \}, \quad \forall i = 1, 2. \end{aligned} \quad (4)$$

Here $\lambda_i = \nabla_{x_i} \vartheta_i$ is the costate of Player i . Solving Eq. (4) for a given initial states in $\mathcal{X} \times [0, T]$ is a boundary-value problem (BVP). Provided that convergence can be achieved, the solution to this BVP approximates ϑ through the resultant characteristic trajectory and the boundary conditions D . Zhang et al. (2023a) uses these characteristic trajectories as supervisory data, but assumes that informative initial states, i.e., those for which c_i changes significantly along the trajectories, are known. PNO exploits the method of characteristics without requiring prior knowledge. See Sec. 4.

4. Pontryagin Neural Operator

PNO is a neural operator $\hat{\vartheta}(\cdot, \cdot, \cdot) : \mathcal{X} \times [0, T] \times \Theta^2 \rightarrow \mathbb{R}$ that maps $\theta \in \Theta^2$ to values of \mathcal{L}^θ . In the following, we first introduce the architecture of PNO and then explain the Pontryagin-mode physics-informed training, which is the key to its success.

Architecture. Following standard treatment in neural operators, we introduce an input function $a(\cdot, \cdot) : \mathcal{X} \times \Theta^2 \rightarrow (0, 1)$ to encode parametric settings of state constraints: $a(\mathbf{x}, \theta) = 1$ if \mathbf{x} violates the constraints according to θ , or otherwise $a(\mathbf{x}, \theta) = 0$. Let $X \in \mathbb{R}^{N \times d_x}$ be a lattice of \mathcal{X} , we denote by $a(X, \theta) \in \{0, 1\}^N$ the batch Boolean outputs at all N lattice nodes. Then $\hat{\vartheta}$ is defined as a linear combination of function bases:

$$\hat{\vartheta}(\mathbf{x}, t, \theta) = \sum_{k=1}^q \underbrace{b_k(a(X, \theta))}_{\text{branch}} \underbrace{t_k(\mathbf{x}, t)}_{\text{trunk}}, \quad (5)$$

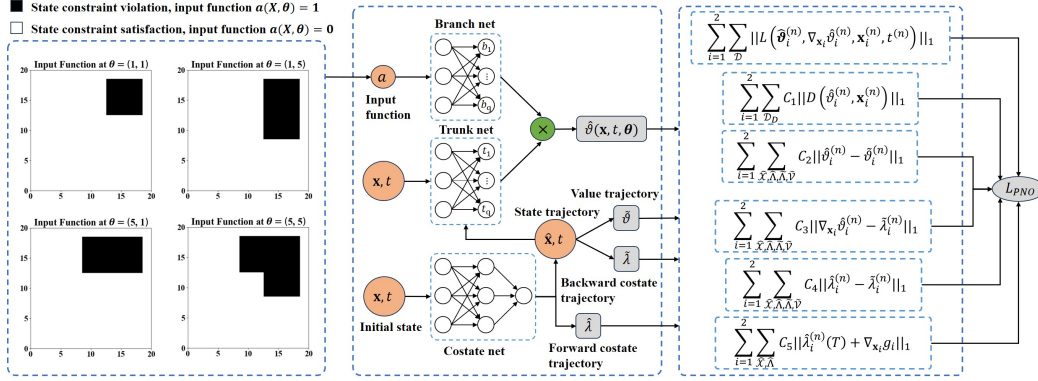


Figure 1: Illustration of Pontryagin Neural Operator. PNO extends DeepONet (Lu et al., 2021) to Pontryagin-mode PINN. The value \hat{v} is decomposed into basis functions (trunk) and their HJI-parameter-dependent coefficients (branch). We use losses on costate predictions to regularize the learning, which is key to the successful learning of values with large Lipschitz constants when state constraints are present. The baseline hybrid neural operator is similar to PNO, but without the learnable costate net. Instead, it solves BVPs as an overhead and use these fixed supervisory data for regularization.

where the branch network $\{b_k\} : \{0, 1\}^N \rightarrow \mathbb{R}$ encodes the PDE parameters into function coefficients, and the trunk network $\{t_k\} : \mathbb{R}^{d_x} \times [0, T] \rightarrow \mathbb{R}$ encodes the input information into basis function values.

Pontryagin-mode PINN. We introduce an additional costate network $\hat{\lambda}(\cdot, \cdot) : \mathcal{X} \times [0, T] \rightarrow \mathcal{X}_*$, where \mathcal{X}_* is the costate space. We can now evaluate the state, costate, and value trajectories starting from some sampled state and time (\mathbf{x}, t) following their corresponding dynamics defined in Eq. (4), first by sequentially maximizing the Hamiltonian using $\hat{\lambda}$ to derive the state trajectory $\hat{\mathbf{x}} \in \mathcal{X}^K$, and then using the transversality conditions of the costate and the value to derive the costate trajectory $\tilde{\lambda} \in \mathcal{X}_*^K$ and the value trajectory $\tilde{v} \in \mathbb{R}^K$ backward in time, where $K = \frac{T-t}{\Delta t}$ and Δt is a small time interval. Given a batch of N initial states, we collect forward state trajectories $\hat{\mathcal{X}} := \{\hat{\mathbf{x}}^{(n)}\}_{n=1}^N$, forward and backward costate trajectories, $\hat{\Lambda} := \{\hat{\lambda}^{(n)}\}_{n=1}^N$ and $\tilde{\Lambda} := \{\tilde{\lambda}^{(n)}\}_{n=1}^N$ respectively, and backward value trajectories $\tilde{\mathcal{V}} := \{\tilde{v}^{(n)}\}_{n=1}^N$. Lastly, we denote the conventional PINN dataset for formulating the PDE and boundary losses as $\mathcal{D} := \{(\mathbf{x}, t)^{(n)} \in \mathcal{X} \times [0, T]\}_{n=1}^{N_D}$ and $\mathcal{D}_D := \{\mathbf{x}^{(n)} \in \mathcal{X}\}_{n=1}^{N_D}$. The PNO training loss with respect to value and costate functions of both players $(\hat{v}, \hat{\lambda})$ is then defined as:

$$\begin{aligned}
 L_{PNO}(\hat{v}, \hat{\lambda}) := & \sum_{i=1}^2 \sum_{\mathcal{D}} \left\| L(\hat{v}_i^{(n)}, \nabla_{\mathbf{x}_i} \hat{v}_i^{(n)}, \mathbf{x}_i^{(n)}, t^{(n)}) \right\|_1 + \sum_{\mathcal{D}_D} C_1 \left\| D(\hat{v}_i^{(n)}, \mathbf{x}_i^{(n)}) \right\|_1 \\
 & + \sum_{\hat{\mathcal{X}}, \hat{\Lambda}, \tilde{\Lambda}, \tilde{\mathcal{V}}} C_2 \left\| \hat{v}_i^{(n)} - \tilde{v}_i^{(n)} \right\|_1 + C_3 \left\| \nabla_{\mathbf{x}_i} \hat{v}_i^{(n)} - \tilde{\lambda}_i^{(n)} \right\|_1 + C_4 \left\| \hat{\lambda}_i^{(n)} - \tilde{\lambda}_i^{(n)} \right\|_1 \\
 & + \sum_{\hat{\mathcal{X}}, \hat{\Lambda}} C_5 \left\| \hat{\lambda}_i^{(n)}(T) + \nabla_{\mathbf{x}_i} g_i \right\|_1,
 \end{aligned} \quad (6)$$

where $\hat{v}_i^{(n)}, \tilde{v}_i^{(n)}, \hat{\lambda}_i^{(n)}, \tilde{\lambda}_i^{(n)}$ are abbreviations for $\hat{v}(\mathbf{x}_i^{(n)}, t^{(n)}, \theta_i^{(n)})$, $\tilde{v}(\mathbf{x}_i^{(n)}, t^{(n)}, \theta_i^{(n)})$, $\hat{\lambda}_i(\mathbf{x}_i^{(n)}, t^{(n)})$, $\tilde{\lambda}_i(\mathbf{x}_i^{(n)}, t^{(n)})$ respectively. $C_i > 0$ for $i = 1, \dots, 5$ are hyperparameters that balance the loss terms. We summarize the training of PNO in Alg. 1. Note that for the Pontryagin-mode losses to be differentiable with respect to $(\hat{v}, \hat{\lambda})$, we use costate net and ODE solver (RK45) to compute the forward and backward trajectories $(\hat{\mathcal{X}}, \hat{\Lambda}, \tilde{\Lambda}, \tilde{\mathcal{V}})$. Line 9-12 in Alg. 1 outline the computation process.

Sampling strategy. For standard PINN residual and boundary datasets \mathcal{D} and \mathcal{D}_D , we use a curriculum learning scheme following (Bansal and Tomlin, 2021; Krishnapriyan et al., 2021) to observe temporal causality of value functions. For Pontryagin-mode trajectories $(\hat{\mathcal{X}}, \hat{\Lambda}, \hat{\Lambda}, \hat{\mathcal{V}})$, our experimental results show that an importance sampling strategy is critical. We start by sampling N initial states uniformly in \mathcal{X} . Subsequently, we follow the evolutionary sampling algorithm (Daw et al., 2022) to compute absolute values of the PDE residual $r(\mathbf{x}_i^{(n)}) = \|L(\hat{\boldsymbol{\vartheta}}_i^{(n)}, \nabla_{\mathbf{x}_i^{(n)}} \hat{\boldsymbol{\vartheta}}_i^{(n)}, \mathbf{x}_i^{(n)}, t^{(n)})\|_1$ for $n = 1, \dots, N$ using Eq. (3). We iteratively sample and remove samples with residuals lower than the average. The resultant batch represents initial states for which the current $\hat{\boldsymbol{\vartheta}}$ cannot generalize well. The sampled initial states gradually accumulate in the region with informative collision and near-collision knowledge during the training. Convergence of the evolutionary-based PINN has been proved in (Daw et al., 2022).

Remarks. PNO does not require offline data collection through solving BVPs and thus avoids typically convergence issues encountered in solving differential games with multiple local equilibria and slow convergence dynamics. While a full PAC learning proof of PNO is not yet available, our results suggest that PNO achieves more data-efficient learning of values and policies than an existing hybrid method that takes advantage of informative samples that reveal structures of the value or costate landscapes. One hypothesis for the success of PNO is that it decomposes the value landscape into (terminal) boundaries and value dynamics along trajectories (a Lagrangian perspective), i.e., the hard-to-learn value with large Lipschitz constant can potentially be learned more effectively when each of its components, namely, the continuous boundary, continuous trajectories, and discontinuous value dynamics, are easy to learn given the others. We note that the improvement in data-efficiency of PINN through the method of characteristics has been discussed in (Mojgani et al., 2023) for 2D convection-diffusion and Burger’s equations, but not yet in the context of high-dimensional HJ equations for optimal control or differential games.

5. Experiments and Results

To demonstrate the efficacy of PNO, we solve HJI equations for the interaction between two vehicles at an uncontrolled intersection. Each vehicle has two state variables (location and velocity) and one parameter that defines their perception of the collision zone. Hence we have a pair of 5D HJI equations defined in a 2D parameter space. We compare PNO with the hybrid method from (Zhang et al., 2023a) using both sample equilibrial trajectories solved from BVP (Eq. (4)) and the value landscape solved by a general-sum extension of the level set algorithm (Bui et al., 2022) (which cannot be scaled to larger problems). Due to space limitation, we will focus on closed-loop safety performance as the performance metric. **Hardware.** Supervised equilibria data and closed-loop intersection simulations are computed on a workstation with 3.50GHz Xeon E5-1620 v4 and one GTX TITAN X with 12 GB memory. Hybrid and Pontryagin neural operators are trained on an A100 GPU with 40 GB memory.

Experiment setup. We adopt settings of the uncontrolled intersection case studied in (Zhang et al., 2023a): Each vehicle is represented by states $x_i := (d_i, v_i)$, d_i for location and v_i for velocity. Both vehicles follow simple dynamics: $\dot{d}_i = v_i$ and $\dot{v}_i = u_i$, where $u_i \in [-5, 10]m/s^2$ is the control input. Let R , L , and W be the road length, vehicle length, and vehicle width, respectively. The instantaneous loss and state constraint are defined as:

$$l_i^\theta(\mathbf{x}_i, u_i) = u_i^2, \quad c_i^\theta(\mathbf{x}_i) = b\sigma(d_i, \theta_i)\sigma(d_{-i}, 1), \quad (7)$$

Algorithm 1: Pontryagin Neural Operator

input : $\mathcal{X}, \mathcal{D}, \mathcal{D}_D, T, \text{pretrain_iters}, \text{train_iters}, \text{gradient_steps}$, learning rate α , network parameters ω
output: $\hat{\vartheta}_\omega, \lambda_\omega$

```

1 initialize branch net  $\{b_k\}$ , trunk net  $\{t_k\}$ , and costate net  $\hat{\lambda}$ 
2  $\mathcal{D}_D \leftarrow$  sample  $\mathbf{x} \in \mathcal{X}$  for  $\{t_k\}$ , and sample  $\mathbf{x} \in \mathcal{X}$  for  $\hat{\lambda}$  at each pretrain iteration
3 pretrain  $\{b_k\}$ ,  $\{t_k\}$ , and  $\hat{\lambda}$  to satisfy value and costate boundary conditions via Eq. (3) and Eq. (4) for pretrain_iters
  iterations
4 set iter = 0, num_epoch = 0
5 while iter  $\leq$  train_iters do
6    $\mathcal{D}_D \leftarrow$  sample  $\mathbf{x} \in \mathcal{X}$  and  $\mathcal{D} \leftarrow$  sample  $\mathbf{x} \in \mathcal{X}$  for  $\{t_k\}$ ; set  $\hat{\Lambda} = \emptyset, \tilde{\Lambda} = \emptyset, \tilde{\mathcal{V}} = \emptyset$ , and  $\hat{\mathcal{X}} = \emptyset$ 
7   if num_epoch mod 10 == 0 then
8      $\mathcal{D} \leftarrow$  sample  $t \in [0, \frac{\text{num\_epoch}+10}{\text{train\_iters}}T]$  for  $\{t_k\}$  /* Increase time window every 10 epochs */
9     sample  $\mathbf{x}(0) \in \mathcal{X}$  for  $\hat{\lambda}$ ;  $\hat{\mathcal{X}} \leftarrow$  compute state trajectories via solving Eq. (4) using  $\hat{\lambda}$ 
10     $\hat{\Lambda} \leftarrow$  compute forward costate trajectories using  $\hat{\lambda}$ 
11     $\tilde{\Lambda} \leftarrow$  compute backward costate trajectories as solutions to inverse value problems with terminal values  $\hat{\mathcal{X}}(T)$  and
       $\hat{\Lambda}(T)$  via solving Eq. (4) using ODE solver (RK45)
12     $\tilde{\mathcal{V}} \leftarrow$  compute value trajectories with  $\hat{\mathcal{X}}$  and  $\tilde{\Lambda}$  via solving Eq. (1) and Eq. (4)
13    num_epoch  $\leftarrow$  num_epoch + 1
14    compute  $L_{PNO}$  via Eq. (6)
15    step = 0
16    while step  $\leq$  gradient_steps do
17       $\omega \leftarrow \omega - \alpha \nabla_\omega L_{PNO}$ 
18      step  $\leftarrow$  step + 1
19    end
20    iter  $\leftarrow$  iter + 1
21 end

```

 Table 1: Safety performance comparison among Hybrid neural operator and PNO, respectively for each parameter configuration in Θ^2 . Ground truth via BVP solver considers inevitable collisions.

Player Types	Learning Method														
Metrics	Ground Truth						Hybrid Neural Operator			Pontryagin Neural Operator					
(θ_1, θ_2) Col. % \downarrow	(1, 1)			(1, 2)			(1, 3)			(1, 4)			(1, 5)		
	0.00%	3.00%	0.33%	2.67%	21.8%	6.50%	4.83%	9.50%	9.17%	9.33%	9.83%	8.00%	9.00%	8.00%	8.17%
	(2, 1)			(2, 2)			(2, 3)			(2, 4)			(2, 5)		
	2.67%	21.8%	6.50%	7.00%	34.7%	8.33%	14.0%	26.3%	15.2%	21.5%	36.2%	21.5%	28.7%	41.5%	26.8%
	(3, 1)			(3, 2)			(3, 3)			(3, 4)			(3, 5)		
	4.83%	9.50%	9.17%	14.0%	26.3%	15.2%	23.7%	22.5%	23.5%	33.3%	32.7%	33.2%	43.0%	41.5%	41.3%
	(4, 1)			(4, 2)			(4, 3)			(4, 4)			(4, 5)		
	9.33%	9.83%	8.00%	21.5%	36.2%	21.5%	33.3%	32.7%	33.2%	42.3%	40.2%	41.3%	54.3%	51.8%	52.3%
	(5, 1)			(5, 2)			(5, 3)			(5, 4)			(5, 5)		
9.00%	8.00%	8.17%	28.7%	41.5%	26.8%	43.0%	41.5%	41.3%	54.3%	51.8%	52.3%	61.0%	60.0%	60.2%	

where

$$\sigma(d, \theta) = (1 + \exp(-\gamma(d - R/2 + \theta W/2)))^{-1} (1 + \exp(\gamma(d - (R + W)/2 - L)))^{-1}. \quad (8)$$

Here shape parameter $\gamma = 5$, and $b = 10^4$ is sufficiently large to prevent collisions. Similar to treating collision as hard constraints, this setting causes the PINN convergence issue. $\theta \in \Theta := \{1, 2, 3, 4, 5\}$ denotes the aggressiveness level (safety preference) of a player. The terminal loss is defined to encourage players to pass the intersection and regain nominal speed:

$$g_i(x_i) = -\mu d_i(T) + (v_i(T) - \bar{v})^2, \quad (9)$$

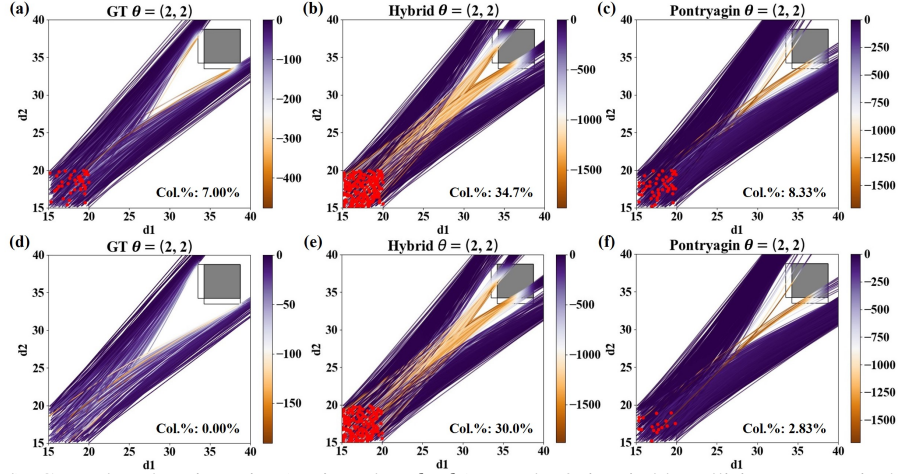
where $\mu = 10^{-6}$, $\bar{v} = 18m/s$, and $T = 3s$.

Data. To demonstrate the advantage of PNO, we perform a comparison in favor of the baseline (the hybrid neural operator): For the baseline, we generate 1k ground truth trajectories from initial states uniformly sampled in $\mathcal{X}_{GT} := [15, 20]m \times [18, 25]m/s$ by solving Eq. (4). This set

Table 2: Safety performance comparison among Hybrid neural operator and PNO, respectively for each parameter configuration in Θ^2 . Ground truth via BVP solver omits inevitable collisions.

Player Types Metrics	Learning Method													
	Ground Truth			Hybrid Neural Operator			Pontryagin Neural Operator							
(θ_1, θ_2) Col.% \downarrow	(1, 1)			(1, 2)			(1, 3)			(1, 4)			(1, 5)	
	0.00%	3.00%	0.33%	0.00%	19.5%	4.33%	0.00%	6.33%	5.67%	0.00%	2.17%	0.00%	0.00%	0.83% 1.00%
	(2, 1)			(2, 2)			(2, 3)			(2, 4)			(2, 5)	
	0.00%	19.5%	4.33%	0.00%	30.0%	2.83%	0.00%	14.7%	3.83%	0.00%	19.0%	1.17%	0.00%	20.2% 0.00%
	(3, 1)			(3, 2)			(3, 3)			(3, 4)			(3, 5)	
	0.00%	6.33%	5.67%	0.00%	14.7%	3.83%	0.00%	0.50%	0.67%	0.00%	1.00%	0.50%	0.00%	1.17% 0.67%
	(4, 1)			(4, 2)			(4, 3)			(4, 4)			(4, 5)	
	0.00%	2.17%	0.00%	0.00%	19.0%	1.17%	0.00%	1.00%	0.50%	0.00%	0.00%	0.00%	0.00%	0.33% 0.33%
	(5, 1)			(5, 2)			(5, 3)			(5, 4)			(5, 5)	
	0.00%	0.83%	1.00%	0.00%	20.2%	0.00%	0.00%	1.17%	0.67%	0.00%	0.33%	0.33%	0.00%	0.00% 0.00%

is identified to contain a significant amount of corner cases (e.g., 61% of \mathcal{X}_{GT} yield collisions when $\theta = (5, 5)$, see Tab. 1) and will also be used for test. Each trajectory consists of 31 data points with a time interval of $0.1s$ for each of the players, resulting in a total of 62k data points. For PNO, the costate net explores the initial state within $\mathcal{X}_{HJ} := [15, 105]m \times [15, 32]m/s$ and generates 1k closed-loop trajectories including 62k data points. \mathcal{X}_{HJ} is much less informed than \mathcal{X}_{GT} . To improve training efficiency, we eliminate data points generated by the costate net that fall beyond the state bounds and normalize the input data to $[-1, 1]$ for the trunk and costate net of both neural operators. Additionally, the trunk net uniformly samples 60k states in $\mathcal{X}_{HJ} := [15, 105]m \times [15, 32]m/s$ for model refinement. Lastly, we train the model using four player-type configurations $(\theta_1, \theta_2) = \{(1, 1), (1, 5), (5, 1), (5, 5)\}$ and evaluate the model generalization performance within the type space Θ . We reiterate that the total number of data points for the two methods are approximately the same.


 Figure 2: (a, d): Ground truth trajectories (projected to d_1 - d_2) w and w/o inevitable collisions, respectively. (b-c), (e-f): Trajectories generated using hybrid and PNO w and w/o inevitable collisions, respectively. Color: Actual values of Player 1. Red dots: Initial states that yield collisions. Solid gray box: collision area for player type $\theta = (1, 1)$.

Training. The neural operators utilize fully-connected networks with 3 hidden layers, each comprising 64 neurons with \tanh activation. The hybrid neural operator uses the Adam optimizer with a fixed learning rate of 2×10^{-5} for pre-training the network over 100k iterations using supervised data. It then combines the supervised data with states sampled from an expanding time window, starting from the terminal time, to refine the model for an additional 100k iterations. PNO uses the Adam optimizer with an adaptive learning rate, starting from 2×10^{-5} , and is initially trained to

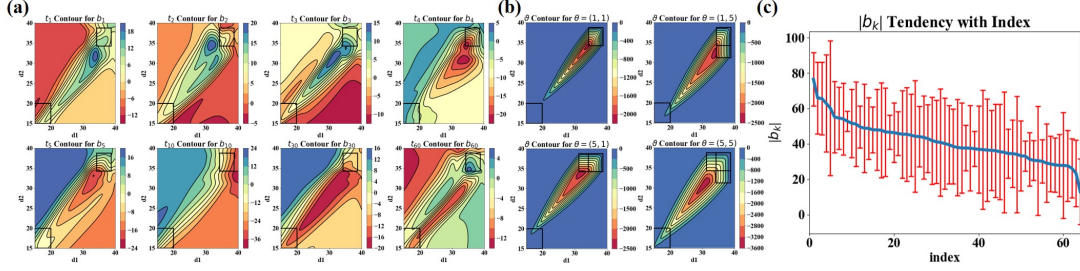


Figure 3: (a) Basis value functions (t_k) corresponding to the largest mean b_k . Visualized for (d_1, d_2) with fixed $v_{1,2} = 18m/s$ and $t = 0$. (b) Ground truth values for sampled θ . (c) Sorted sample mean and std of coefficients $|b_k|$ over Θ^2 .

satisfy the boundary conditions over 50k iterations. Subsequently, the network undergoes refinement through 3k gradient steps per epoch, encompassing a total of 10 epochs for every 10 training iterations. The costate net resamples the initial state to generate closed-loop trajectories every 10 epochs, and these data points are used to train the model. The overall network refinement process spans 300 training iterations. Both PNO and hybrid incorporate adaptive activation functions (Jagtap et al., 2020). In terms of wall-clock computational cost, the hybrid neural operator requires approximately 37 hours, including 5.5 hours for data acquisition and 31.5 hours for model training. PNO requires 27 hours for model training. For comparison, solving all 25 individual HJI PDEs in Θ^2 with an acceptable meshgrid resolution using an efficient level set package (Bui et al., 2022) would require > 50 hours. The resultant value approximation does not guarantee safety performance since value gradient approximation error is not controlled.

Safety performance. We use the neural operators for closed-loop control on test cases uniformly sampled in \mathcal{X}_{GT} and report their safety performance in percentage of collisions, where collisions are defined by θ . For better transparency, the comparison uses two sets of ground truth trajectories: The first contains 600 trajectories for each parameter configuration in Θ^2 ; the second uses the same setting but only contains trajectories without physical collisions (for initial states from which collision cannot be avoided according to $\theta = (1, 1)$). Tab. 1 and Tab. 2 summarize safety performance comparisons with and without inevitable collisions, generalizing to testing cases across Θ^2 . The results show that PNO outperforms the hybrid neural operator in most cases. More importantly, it achieves this without relying on domain knowledge (informative trajectories in \mathcal{X}_{GT}). Trajectories from test player types are visualized in Fig. 2. It should be noted that in some cases neural operators perform better than the ground truth. This is because a multi-start BVP solver solves the ground truth trajectories with heuristic initial guesses. We also note that while BVP solutions are open-loop, their corresponding values are consistent with the HJI equations for this case study (see comparison between BVP and HJI value contours at $t = 0$ in Fig. 4).

Structure of parametric value. Since branch and trunk nets learn a decomposition of the value function in the parameter space, Fig. 3 investigates the learned value structure through visualization of (1) the major basis value functions associated with the largest sample means of coefficients (b_k in Eq. (5)) over Θ^2 (Fig. 3a), (2) the ground truth values solved using level set for $\theta = (1, 1)$, $(1, 5)$, $(5, 1)$, $(5, 5)$ (Fig. 3b), and (3) the sorted mean and standard deviation of absolute coefficients (Fig. 3c). We see that the major bases the mean and major variances of the value over Θ^2 well. Further regularization on the branch net to promote basis sparsity and extension of existing generalization results to neural operators are worth investigating in future studies.

Ablation studies. Due to the reported importance of activation choice in PINN, we report ablation studies to understand the influence of activation on safety performance. Tab. 3 summarize the safety

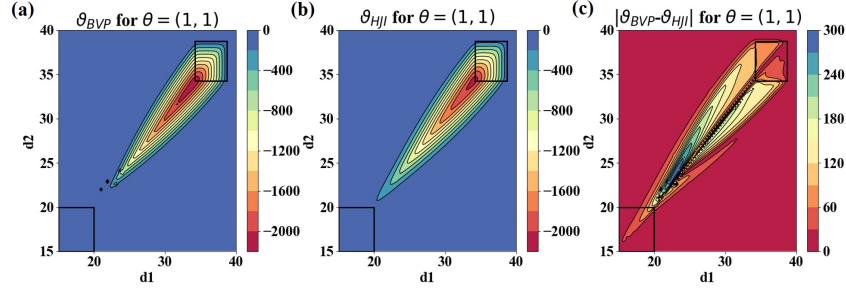


Figure 4: (a, b) Value contour of BVP solutions and HJI equations projected on (d_1, d_2) with fixed $v_{1,2} = 18m/s$ and $t = 0$ for given $\theta = (1, 1)$, respectively. (c) Difference $|\vartheta_{BVP} - \vartheta_{HJI}|$ is visualized for d_1-d_2 .

performance using different activation functions for comparisons w/ and w/o inevitable collisions. The comparison of closed-loop trajectories is visualized in Fig. 5. The results show that the choice of activation significantly affects the model performance: `tanh` outperforms `sine` and `relu`.

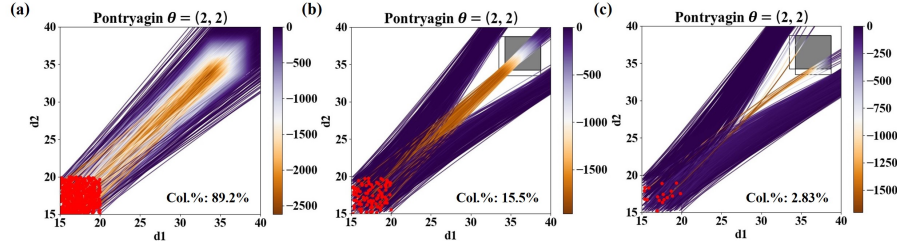


Figure 5: Closed-loop trajectories generated using PNO with (a) `relu`, (b) `sine` and (c) `tanh` activation functions without inevitable collisions.

Table 3: Safety performance comparison among different activation functions using PNO without inevitable collisions for each parameter configuration in Θ^2

Player Types		Activation Function											
Metrics		relu			sine			tanh					
(θ_1, θ_2) Col.% ↓	(1, 1)	81.3%	1.83%	0.33%	(1, 2)	84.8%	4.33%	4.33%	(1, 3)	86.2%	12.5%	5.67%	
	(2, 1)	84.8%	4.33%	4.33%	(2, 2)	89.2%	15.5%	2.83%	(2, 3)	88.8%	12.0%	3.83%	
	(3, 1)	86.2%	12.5%	5.67%	(3, 2)	88.8%	12.0%	3.83%	(3, 3)	92.5%	4.17%	0.67%	
	(4, 1)	86.8%	5.33%	0.00%	(4, 2)	90.3%	4.33%	1.17%	(4, 3)	91.5%	0.83%	0.50%	
	(5, 1)	87.8%	3.50%	1.00%	(5, 2)	89.8%	0.67%	0.00%	(5, 3)	93.7%	0.67%	0.67%	
	(1, 4)	86.8%	5.33%	0.00%	(1, 5)	87.8%	3.50%	1.00%	(2, 4)	90.3%	4.33%	1.17%	
	(2, 4)	89.8%	0.67%	0.00%	(2, 5)	89.8%	0.67%	0.00%	(3, 4)	91.5%	0.83%	0.50%	
	(3, 4)	93.7%	0.67%	0.67%	(3, 5)	93.7%	0.67%	0.67%	(4, 4)	94.8%	0.33%	0.00%	
	(4, 4)	95.3%	0.17%	0.33%	(4, 5)	95.3%	0.17%	0.33%	(5, 4)	95.3%	0.17%	0.33%	
	(5, 4)	95.8%	0.00%	0.00%	(5, 5)	95.8%	0.00%	0.00%	(5, 5)	95.8%	0.00%	0.00%	

6. Conclusion

We introduced PNO to approximate parametric value functions with large Lipschitz constants as solutions to two-player general-sum differential games. Compared with the existing solution that requires informative supervisory data, PNO is fully self-supervised and free of prior knowledge about corner cases. For this reason, PNO is also free of convergence issues related to the existence of multiple equilibria or singular arcs in solving BVPs. In a case study involving two vehicles interacting at an uncontrolled intersection, our numerical results demonstrated that PNO yields superior safety performance compared to the hybrid neural operator, achieving this with a lower computational cost. The key ingredients of PNO are the self-supervised costate losses that align the learned values and value gradients with the discontinuous value dynamics governed by PMP, and the evolutionary sampling strategy that reveals informative state-space regions during the learning.

Acknowledgments

This work was in part supported by NSF CMMI-1925403 and NSF CNS-2101052. The views and conclusions contained in this document are those of the authors and should not be interpreted as representing the official policies, either expressed or implied, of the National Science Foundation or the U.S. Government.

References

- Somil Bansal and Claire J Tomlin. DeepReach: A deep learning approach to high-dimensional reachability. In *2021 IEEE International Conference on Robotics and Automation (ICRA)*, pages 1817–1824. IEEE, 2021.
- Minh Bui, George Giovanis, Mo Chen, and Arrvindh Shriraman. Optimizeddp: An efficient, user-friendly library for optimal control and dynamic programming. *arXiv preprint arXiv:2204.05520*, 2022.
- Pierre Cardaliaguet. Information issues in differential game theory. In *ESAIM: Proceedings*, volume 35, pages 1–13. EDP Sciences, 2012.
- Michael G Crandall and Pierre-Louis Lions. Viscosity solutions of hamilton-jacobi equations. *Transactions of the American mathematical society*, 277(1):1–42, 1983.
- Arka Daw, Jie Bu, Sifan Wang, Paris Perdikaris, and Anuj Karpatne. Mitigating propagation failures in pinns using evolutionary sampling. 2022.
- Jaime F Fisac, Mo Chen, Claire J Tomlin, and S Shankar Sastry. Reach-avoid problems with time-varying dynamics, targets and constraints. In *Proceedings of the 18th international conference on hybrid systems: computation and control*, pages 11–20, 2015.
- Nidhal Gammoudi and Hasnaa Zidani. A differential game control problem with state constraints. *Mathematical Control and Related Fields*, 13(2):554–582, 2023.
- Jiequn Han and Jihao Long. Convergence of the deep bsde method for coupled fbsdes. *Probability, Uncertainty and Quantitative Risk*, 5(1):1–33, 2020.
- Jiequn Han, Arnulf Jentzen, and Weinan E. Solving high-dimensional partial differential equations using deep learning. *Proceedings of the National Academy of Sciences*, 115(34):8505–8510, 2018.
- Zhongkai Hao, Zhengyi Wang, Hang Su, Chengyang Ying, Yinpeng Dong, Songming Liu, Ze Cheng, Jian Song, and Jun Zhu. Gnot: A general neural operator transformer for operator learning. In *International Conference on Machine Learning*, pages 12556–12569. PMLR, 2023.
- Kazufumi Ito, Christoph Reisinger, and Yufei Zhang. A neural network-based policy iteration algorithm with global h2-superlinear convergence for stochastic games on domains. *Foundations of Computational Mathematics*, 21(2):331–374, 2021.

- Ameya D Jagtap, Kenji Kawaguchi, and George Em Karniadakis. Adaptive activation functions accelerate convergence in deep and physics-informed neural networks. *Journal of Computational Physics*, 404:109136, 2020.
- Nikola Kovachki, Zongyi Li, Burigede Liu, Kamyar Azizzadenesheli, Kaushik Bhattacharya, Andrew Stuart, and Anima Anandkumar. Neural operator: Learning maps between function spaces with applications to pdes. *Journal of Machine Learning Research*, 24(89):1–97, 2023.
- Aditi Krishnapriyan, Amir Gholami, Shandian Zhe, Robert Kirby, and Michael W Mahoney. Characterizing possible failure modes in physics-informed neural networks. *Advances in Neural Information Processing Systems*, 34:26548–26560, 2021.
- Zongyi Li, Nikola Kovachki, Kamyar Azizzadenesheli, Burigede Liu, Kaushik Bhattacharya, Andrew Stuart, and Anima Anandkumar. Fourier neural operator for parametric partial differential equations. *arXiv preprint arXiv:2010.08895*, 2020.
- Lu Lu, Pengzhan Jin, Guofei Pang, Zhongqiang Zhang, and George Em Karniadakis. Learning nonlinear operators via deepnet based on the universal approximation theorem of operators. *Nature machine intelligence*, 3(3):218–229, 2021.
- Olvi L Mangasarian. Sufficient conditions for the optimal control of nonlinear systems. *SIAM Journal on control*, 4(1):139–152, 1966.
- Ian M Mitchell and Jeremy A Templeton. A toolbox of Hamilton-Jacobi solvers for analysis of nondeterministic continuous and hybrid systems. In *Hybrid Systems: Computation and Control: 8th International Workshop, HSCC 2005, Zurich, Switzerland, March 9-11, 2005. Proceedings 8*, pages 480–494. Springer, 2005.
- Rambod Mojtani, Maciej Balajewicz, and Pedram Hassanzadeh. Kolmogorov n-width and lagrangian physics-informed neural networks: a causality-conforming manifold for convection-dominated pdes. *Computer Methods in Applied Mechanics and Engineering*, 404:115810, 2023.
- Tenavi Nakamura-Zimmerer, Qi Gong, and Wei Kang. Adaptive deep learning for high-dimensional hamilton-jacobi-bellman equations. *SIAM Journal on Scientific Computing*, 43(2):A1221–A1247, 2021.
- Stanley Osher and Chi-Wang Shu. High-order essentially nonoscillatory schemes for Hamilton-Jacobi equations. *SIAM Journal on numerical analysis*, 28(4):907–922, 1991.
- Stanley Osher, Ronald Fedkiw, and K Piechor. Level set methods and dynamic implicit surfaces. *Appl. Mech. Rev.*, 57(3):B15–B15, 2004.
- Julien Pérolat, Florian Strub, Bilal Piot, and Olivier Pietquin. Learning nash equilibrium for general-sum markov games from batch data. In *Artificial Intelligence and Statistics*, pages 232–241. PMLR, 2017.
- Yeonjong Shin, Jerome Darbon, and George Em Karniadakis. On the convergence of physics informed neural networks for linear second-order elliptic and parabolic type pdes. *arXiv preprint arXiv:2004.01806*, 2020.

- Alan Wilbor Starr and Yu-Chi Ho. Nonzero-sum differential games. *Journal of optimization theory and applications*, 3(3):184–206, 1969.
- Sifan Wang, Hanwen Wang, and Paris Perdikaris. Learning the solution operator of parametric partial differential equations with physics-informed deepnets. *Science advances*, 7(40):eabi8605, 2021.
- E Weinan, Jiequn Han, and Arnulf Jentzen. Algorithms for solving high dimensional PDEs: from nonlinear Monte Carlo to machine learning. *Nonlinearity*, 35(1):278, 2021.
- Jeremy Yu, Lu Lu, Xuhui Meng, and George Em Karniadakis. Gradient-enhanced physics-informed neural networks for forward and inverse pde problems. *Computer Methods in Applied Mechanics and Engineering*, 393:114823, 2022.
- Lei Zhang, Mukesh Ghimire, Wenlong Zhang, Zhe Xu, and Yi Ren. Approximating discontinuous nash equilibrial values of two-player general-sum differential games. In *2023 IEEE International Conference on Robotics and Automation (ICRA)*, pages 3022–3028. IEEE, 2023a.
- Lei Zhang, Mukesh Ghimire, Wenlong Zhang, Zhe Xu, and Yi Ren. Value approximation for two-player general-sum differential games with state constraints, 2023b.